Pergamon

Journal of Structural Geology, Vol. 17, No. 1, pp. 31 to 45, 1995

0191-8141/95 $9.50 + 0.00

0191-8141(94)E0031-S

Kinematics and a balanced and restored cross-section across the toe of the eastern Nankai accretionary prism

J. K. MORGAN and D. E. KARIG

Department of Geological Sciences, Cornell University, Ithaca, NY 14853-1504, U.S.A.

(*Received* 25 *March* 1993; *accepted in revised form* 13 *February* 1994)

Abstract—Seismic profiles across the eastern Nankai accretionary prism show evidence for diffuse deformation through stratal thickening and uplift of the accreting sediment package, thought to reflect the combination of small-scale ductile and brittle strains evident within drill cores. Using a kinematic solution based on changes in stratal thickness and porosities, diffuse strains are estimated for a transect across the eastern Nankai accretionary prism toe, in the vicinity of ODP Site 808. Calculated element displacements are used to reconstruct the undeformed configuration of the prism toe, providing a new method for balancing and restoring deformation in accretionary prisms.

The results of this analysis demonstrate a heterogeneous distribution of strain within the prism toe, which appears to correlate with the distribution of brittle deformation structures in drill cores. The greatest vertical tectonic thickening and horizontal shortening estimates are obtained within the deepest sediments, which also display abundant brittle shears. Shallower sediments exhibit high volume loss and lower horizontal shortening, and in drill cores display very few deformation structures. This spatially variable strain distribution may result from inferred high pore pressures near the frontal thrust and décollement inducing a brittle overprint of previous ductile strains.

INTRODUCTION

The Nankai Trough and accretionary prism, off the southeast coast of Japan, have been the focus of extensive study in recent years, including several ocean drilling cruises (Karig *et al.* 1975, Kagami *et al.* 1985, Taira *et al.* 1991) and seismic surveys (e.g. Moore *et al.* 1990). As a result of these efforts, we have a relatively good understanding of the stratigraphic and structural framework of the active trench and prism. In addition, there exists a large compilation of physical properties, structural, and chemical data derived from drill cores, from which we have been able to infer much regarding processes active in the prism toe. Despite this extensive data base, it has proven very difficult to estimate the state of strain within the Nankai prism toe. Diffuse internal strain, evident from the thickening of the accreted sediments on the seismic profiles and attributed to distributed ductile and small-scale brittle deformation, is thought to be an important contributor to the total strain state, but this quantity remains difficult to measure directly.

A new technique for estimating the diffuse strain field in accretionary prism toes was recently proposed by Morgan *et al.* (1994), which integrates porosities, measured in the drill cores and estimated from seismic interval velocities, and distortional strains indicated by changes in bed thickness on seismic depth profiles. This unique kinematic approach involves a compact solution to the Lagrangian conservation of mass equation, aided by approximately steady-state deposition and accretion to the prism toe. The method was applied to an unfaulted but tectonically deformed section of the Nankai accretionary prism in the vicinity of Deep Sea Drilling Project (DSDP) Sites 298, 582 and 583 (western transect). That effort yielded first-order estimates for a heterogeneous diffuse strain field which appears to depend primarily on the consolidation state of the sediment at the time of accretion (Morgan *et al.* 1994).

In this paper, we concentrate on a parallel transect across the Nankai Trough and prism in the vicinity of Ocean Drilling Program (ODP) Site 808, about 100 km northeast of the previous section. The kinematic solution is applied to the three most seaward domains within the prism: the protothrust zone and the first two thrust sheets. Although porosities and seismic interval velocities along this transect are less well constrained than along the western transect, a limiting solution for the diffuse strains which minimizes volume change and horizontal shortening can be derived from the available data. In this way, the general shape of the strain distribution can be examined, and compared across domain boundaries. Once reasonable estimates for the distribution of diffuse strain within the deformed domains are obtained, the undeformed configuration of the prism toe can be reconstructed and the magnitudes of shortening due to diffuse internal strain and displacement along thrust faults can be compared.

Although diffuse strains determined in this analysis cannot be directly broken down into their ductile and brittle components, the excellent data set derived from ODP Site 808 may permit core scale structures and fabrics to be correlated with the diffuse strain field. Preliminary estimates regarding the relative importance of ductile and brittle modes of deformation and the volumetric contribution to strain can be made from this comparison, and the likely progression of deformation predicted. Moreover, with the results of Leg 131 post-

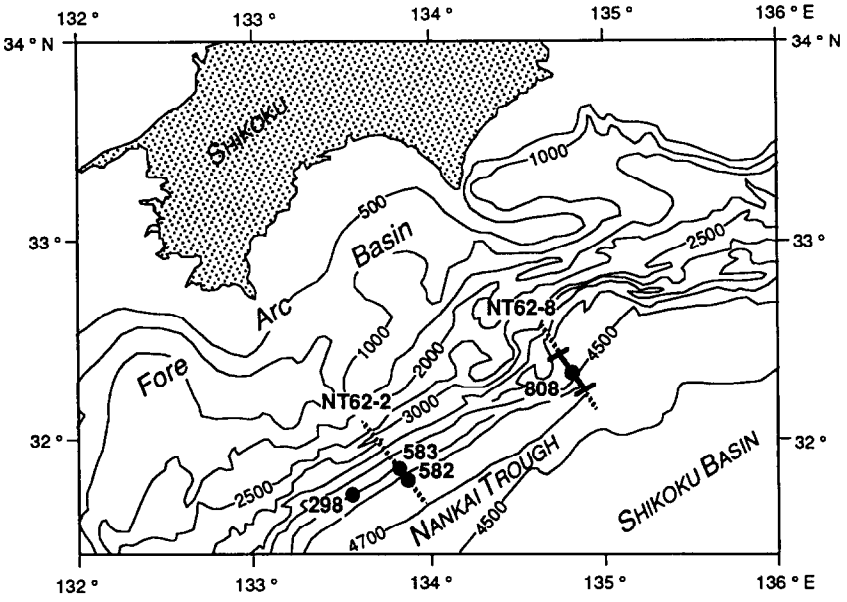

Fig. 1. Bathymetric map of the Nankai accretionary margin. The locations of DSDP Sites 298, 582 and 583 and ODP Site 808 are marked, along with the traces of two seismic profiles, NT62-2 and NT62-8 along the western and eastern transects across the prism toe respectively. The portion of NT62-8 shown in Fig. 2(a) is bracketed.

cruise studies in hand (Hill *et al.* 1993), we can begin to infer the important mechanical and hydrologic processes active in the prism toe, and consider their influence on the mode and magnitude of deformation during accretion.

TECTONIC SETTING AND PRISM GEOMETRY

The Nankai convergent margin lies at the boundary between the Eurasian and Philippine Sea plates, off the southeast coast of Japan (Fig. 1). The inactive Shikoku back-arc basin and overlying sediments are presently being subducted northwestward with a time-averaged, relative convergence rate of 2 cm y^{-1} perpendicular to the strike of the margin (Karig & Angevine 1985). The boundary is marked by the Nankai Trough, and a landward sequence of linear ridges and troughs of the imbricate stack of thrust sheets at the toe of the accretionary prism.

The eastern section of the Nankai Trough and prism is transected by seismic depth profile, NT62-8 (Fig. 2a, from Moore *et al.* 1990). The good seismic coherence and relatively good velocity control obtained through a series of two-ship seismic experiments (Stoffa *et al.* 1992), permit identification and correlation of continuous stratal reflections within the trench, and into the first two thrust sheets. The stratigraphic and structural interpretations are calibrated by the data from ODP Hole 808C, which penetrated the leading edge of the first thrust sheet and the unfaulted footwall strata beneath the frontal thrust, and extended through the basal décollement, the subducting sediments, and into the oceanic crust (Fig. 2b).

Two distinct stratigraphic packages can be distinguished on the seismic profile. The Shikoku Basin hemipelagic sediments overlie and nearly parallel the NW-dipping, subducting ocean crust. Onlapping the dipping basin strata are the sub-horizontal hemipelagic muds and turbidites of the trench fill. The contact between the Shikoku Basin sequence and the trench fill strata represents a facies boundary marking the lateral position of the outer trench margin. This time-transgressive contact is observed to cut down-section in the arcward direction, reflecting progressively shorter accumulation times for the Shikoku Basin deposits (Bray & Karig 1988). Irregular onlap relationships at this boundary indicate that the position of the outer trench margin varied through time, such that the facies boundary is often difficult to trace. Several sharp reflectors on the seismic profile which lie beneath the onlapping trench fill (Fig. 2a) correspond to the basin–trench transition within Hole 808 and a sudden drop in the sediment accumulation rate (Taira *et al.* 1991). For our purposes, the facies boundary is chosen as the lowermost reflector in this set (Fig. 2b).

The basal décollement lies within the Shikoku Basin sequence at a constant stratigraphic horizon as far as can be traced beneath the prism toe (Fig. 2). The onset of diffuse deformation in the overlying accreting trench fill and basin sediments is evident by the slight uplift and seaward tilting of reflectors at a poorly defined deformation front, observed well in front of the frontal thrust faults. The accreting package thickens slightly within the 'protothrust zone' (PTZ) which lies between the first thrust fault and the deformation front. In contrast, the subducting sediment package shows little evidence of deformation, and does not change thickness significantly arcward of the deformation front.

Several prominent faults rise from the décollement, bounding the first and second thrust sheets (TS1 and TS2, respectively). The facies boundary reflectors are

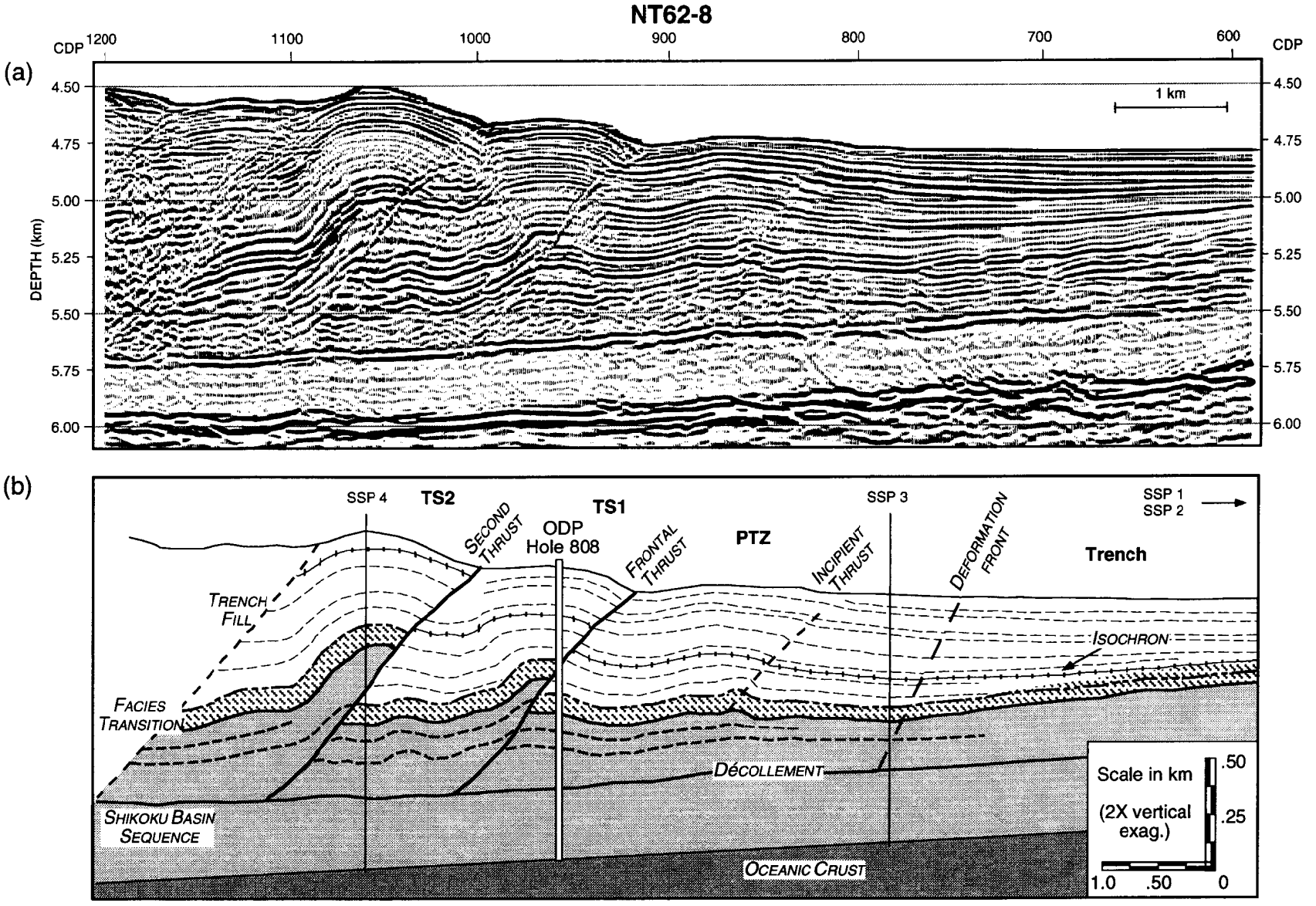

Fig. 2. Seismic profile NT62-8 across the Nankai Trough and prism. (a) A portion of seismic profile NT62-8 across the eastern transect of the Nankai Trough and prism (position indicated in Fig. 1), presented as a depth section with 2:1 vertical exaggeration (adapted from Moore *et al.* 1990). (b) Interpreted depth section at 2:1 vertical exaggeration. Prominent reflectors correlated within the protothrust zone (PTZ), first, and second thrust sheets (TS1 and TS2, respectively) are shown by dashed lines. Trench fill sediments are white, facies transition is dashed, and the Shikoku Basin sediments are shown in dark gray. The hachured line within the trench and prism toe represents an isochron which appears to cross the facies boundary. The locations of ODP Hole 808 and several split spread profiles (SSPs) are also indicated.

displaced about 350 m across the second thrust; the 150 m displacement across the frontal thrust is verified by the repetition of a distinctive pebble-conglomerate bed within Hole 808C (Taira *et al.* 1991). Displacements along the fault lengths are not constant, but rather decrease both upwards and downwards from the center. An incipient thrust fault within the protothrust zone displays features similar to the arcward faults, specifically a reverse sense of displacement, variable offset along its length, and the slight uplift of trench-fill strata in the hangingwall.

The correlation of seismic reflectors within the prism toe (Fig. 2) is complicated by lateral changes in seismic coherence and amplitude, as well as changes in stratal thickness across thrust faults. In addition, the sudden loss of several upper reflectors, and the thinning of the trench-fill package across thrust faults points to significant erosion of the uplifted thrust sheets (e.g. Moore *et al.* 1991); up to 100 m of material is missing in the first thrust sheet, and nearly 200 m in the second. The disturbed deposits at the top of Hole 808C (Taira *et al.* 1991) must be the result of downslope remobilization of surficial sediments, an interpretation supported by the presence of lobes of slumped material on the IZANAGI seafloor images (see Shipboard Scientific Party 1991, Fig. 6). The unconsolidated submarine sediments found at the surface are typically very mobile, and tend to slide seaward when even mildly tilted (Kastens *et al.* 1992).

The folded strata in the hangingwall of the thrust faults qualitatively resemble classic fault-bend folds that form above thrust ramps (Suppe 1983). However they deviate from standard geometries in several respects. The bed-normal thicknesses of the strata generally increase arcward within the thrust sheets, documenting a component of diffuse strain within the thrust sheets probably acquired prior to thrusting. The kink planes are poorly defined within the thrust sheets, and they tend to dip more shallowly than classic kink planes which bisect the angle between the ramp and flat (décollement). Their dips may have been modified by diffuse internal strain of the deformed thrust sheet (e.g. Moore *et al.* 1991), or alternatively the strata may have been broadly folded prior to thrusting. This is supported by the presence of uplifted and folded Shikoku Basin strata in the footwall of the first thrust as well at the base of the incipient thrust within the PTZ. Other complications, such as the up-ramp increase in bed dip and the non-parallel kink planes, may arise from the listric geometry of the thrust faults. Such geometric anomalies and the occurrence of diffuse internal strain and volume change complicate the balancing of the prism toe using the standard bed length or area balancing methods (Woodward *et al.* 1985).

INGREDIENTS OF DIFFUSE DEFORMATION

The diffuse thickening of stata on seismic profiles along the transects across the Nankai prism toe reflects distributed brittle and ductile deformation, which can be recognized and discriminated in core-scale structures and deformation fabrics identified at ODP Site 808. Certainly the most ubiquitous deformation structures observed in the drill cores were brittle microfaults which generally showed a reverse sense of displacement (Taira *et al.* 1991, Maltman *et al.* 1993). These were heterogeneously distributed, nearly absent near the top of the section and increasing in abundance below the frontal thrust to the décollement. Semi-brittle deformation bands, previously described at DSDP Site 583 by Karig & Lundberg (1990), appeared to be symmetrically distributed about and possibly genetically related to the frontal thrust (Taira *et al.* 1991). Where the two features occur together, the microfaults generally overprint the deformation bands.

In addition to brittle and semi-brittle deformation structures, ductile (i.e. plastic) modes of strain are believed to contribute to the total diffuse deformation. Indicators of pervasive ductile strain include changes in sediment porosities and mineral preferred orientation. At the stresses predicted for accretionary prism toes, strain and porosity reduction are assumed to be accommodated by the mechanical reorientation and improved packing of sediment elements, particularly clay minerals (e.g. grain boundary sliding, Borradaile 1981, Maltman 1984). Although decreasing porosities with depth at ODP Site 808 are most easily explained by normal consolidation (Taira *et al.* 1991), an arcward reduction in porosity attributed to tectonic strains (Bray & Karig 1985) may also be important here. Tectonically modified mineral fabrics which might accompany such ductile tectonic deformation have been documented above the décollement in Hole 808C (Byrne *et al.* 1993, Morgan & Karig 1993, Owens 1993).

The timing of the disparate ductile and brittle modes of deformation and their relative contributions to the total deformation are not well understood, but the observations and analyses performed on cores from Site 808, and the estimation of diffuse strains using this kinematic solution now permit these quantities to be related. It may be possible to correlate the core-scale structures and fabrics with diffuse strain estimates, and make some inferences about the mechanics of deformation within the prism toe.

KINEMATIC MODEL AND SOLUTION

The most common description for the deformation field in geologically deformed terrains is one in which the strain is given as a function of position. This Eulerian (or spatial) description is attractive because we can often examine only the deformed state of the material, and must infer the undeformed position or condition. The weakness of this description is that it incompletely describes the progressive changes an individual element experiences as it moves through the Eulerian field. A Lagrangian (or material) description of deformation, wherein strains are tracked along trajectories, is more relevant to understanding the material response to tec-

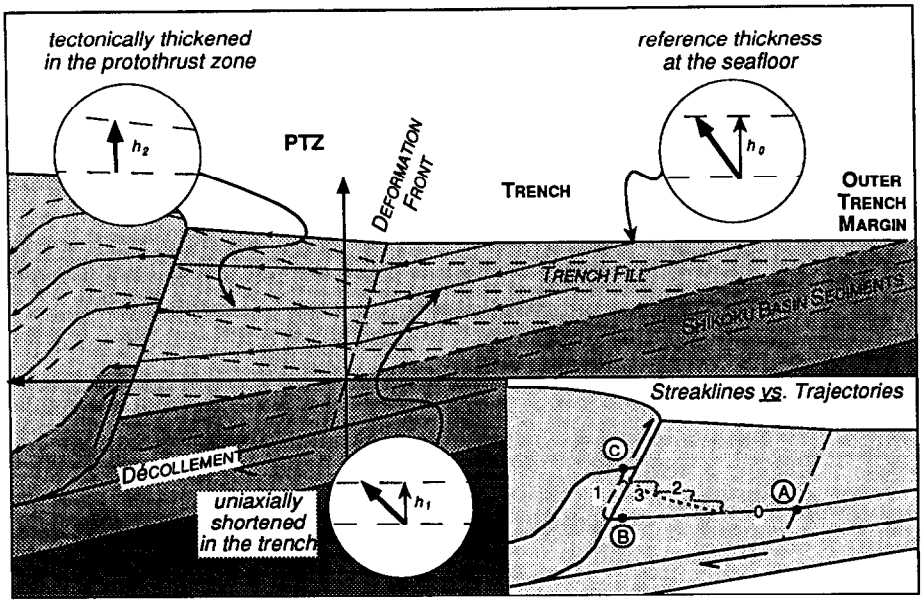

Fig. 3. Steady-state, two-dimensional model deposition and initial accretion along the eastern Nankai accretionary prism. Bedding plane reflectors (dashed lines) are horizontal in the trench and onlap dipping reflectors in the Shikoku Basin sequence. Within the protothrust zone (PTZ), reflectors terminate at the seafloor, marking uplift and drop in sedimentation rate at the deformation front. Sediments are simultaneously buried in the trench and carried arcward relative to the deformation front, following 'paths' (i.e. streaklines) subparallel to the dipping Shikoku Basin strata, but oblique to the trend of the trench-fill reflectors, which migrate passively with the accreting sediments. At the deformation front, the streaklines diverge; the lowermost is parallel to the décollement and the uppermost is subparallel to the seafloor. The vertical dimension of an accreting element (bold arrows) changes along sediment streaklines during deformation; this can be approximated by the vertical spacing between stratigraphic reflectors, h_0, h_1 and h_2. The inset shows the difference between element streaklines and trajectories. Elements at points B and C both passed through point A along the deformation front, as did all the points along the streakline indicated by the solid line. The element at B may have followed a trajectory that follows the streaklines through the deformation front. However, the element at C has been displaced along the thrust fault, and the trajectory taken depends on the history of displacement: recent instantaneous displacement would result in trajectory 1; episodic displacement might lead to trajectory 2; smooth and continuous displacement might result in trajectory 3. Note that element trajectories are continuous while particle streaklines are discontinuous across the thrust fault.

tonic stresses (Karig 1990). A nearly steady-state system, in which both the deformed and undeformed material states can be examined, is most conducive to a Lagrangian strain calculation.

Demonstrating that compensating changes in subduction rate and sediment supply maintained a nearly constant trench and deformation front geometry for the last 10^6 y, Karig & Angevine (1985) argued that deposition and initial accretion at the Nankai margin can be treated as approximately steady-state processes. A simple two-dimensional steady-state model based on this assumption is proposed in Fig. 3. Infinitesimal elements of sediment deposited on the trench or basin floor are carried arcward with the subducting plate during burial, following trajectories that approximately parallel bedding in the Shikoku Basin strata. In the trench fill, element trajectories apparently cross the trend of bedding reflectors, as the later represent passive markers that move with the elements as they are buried and carried arcward. At the deformation front, the element trajectories diverge as sediments tectonically deform. Sediment elements change volume and shape along their trajectories during burial and accretion, acquiring finite strain states defined by their positions within the prism. Decomposing this finite strain along the trajectory permits the progressive strain history of the element to be determined.

Several features within the toe of the prism indicate the breakdown in true steady-state conditions. Thrust faults represent discontinuities in the prism that migrate with the accreting sediments. Folds within the prism also travel through the reference frame, possibly evolving as they move. These introduce complex element trajectories which depend on poorly known uplift and displacement histories of the accreting sediments. For this reason, accurately determining the progressive finite strain of a sediment element may not be possible.

However, the finite strain accrued by an accreting element can be estimated if that element can be projected back to some known steady-state condition. With the help of the bedding reflectors, we can create a map of the current positions of all elements that passed through a single point in that reference configuration, yielding a 'streakline' (e.g. Peerless 1967). This differs from an element trajectory (pathline), which represents the exact path taken by a given element from the reference point to its present position (Fig. 3). In our analysis, a streakline is most conveniently defined by the point it intersects along the deformation front, which in turn is ascribed a vertical co-ordinate relative to the décolle-

ment surface (or displacement). Although we have argued for an approximately steady-state system for deposition and initial accretion, these conditions are not fixed requirements. Changes in the thickness of the accreting sediment package or the subsequent erosion of strata will be indicated by incomplete streaklines which transect the upper surface of the prism.

The kinematic method presented by Morgan *et al.* (1994) offers a compact approach for defining material deformation through a solution of the Lagrangian form of the conservation of mass equation, using the finite element method. The numerical solution entails a two-part calculation for element streaklines and ultimately the finite strain field. While the presence of faults and folds prevents calculation of exact progressive strains, finite strain increments can be estimated, from which the non-tectonic (consolidation) and tectonic stages of deformation can be decomposed. The nature of the solution guarantees strain compatibility within continuously deforming domains, avoiding a problem encountered when performing graphic reconstructions.

Briefly, the finite strain state, which is described most completely by the deformation gradient tensor, **F**, or equivalently by its inverse $\mathbf{F}^{-1}$, can be calculated from vertical thickness ratios and volume ratios, quantities that can be estimated from seismic and physical properties data. The vertical thickness ratio relates the vertical dimension of a line element in the prism to that of the same line element in some undeformed reference configuration. These dimensions are approximated respectively by the vertical spacing between reflectors in the prism, h_2 and the spacing between the same reflectors at the deformation front, h_1 (Fig. 3). Correcting for uniaxial shortening during burial determined from porosity changes gives the vertical thickness ratios, h_2/h_0, which represents one component of the inverse deformation gradient.

The volume ratio, V_2/V_0, describes the volumetric change between the deformed and undeformed configurations, and assuming constant grain density within the accreting sediments, this quantity is equivalent to the determinant of the deformation gradient tensor, **F**. This relationship can be inverted to yield the inverse form of the Lagrangian conservation of mass equation:

$$V_0/V_2 = \det \mathbf{F}^{-1}, \quad (1)$$

thereby relating vertical thickness ratios and volume ratios. Given unique distributions of input ratios, and boundary conditions defined by element displacements along the seaward boundary of the deforming domain and along the décollement (also a streakline), this equation can be solved for the components of **F**. The boundary displacements for each successive domain are given by the displacements obtained for the previous seaward domain along the intervening boundary.

As the input ratios are not well represented by continuous analytical functions within the prism, rectilinear meshes are superimposed on the three tectonically deformed domains (PTZ, TS1, TS2), and the input ratios are discretized at the element nodes. The finite element method is then used to calculate the total deformation gradient field.

STRAIN CALCULATIONS ALONG THE EASTERN TRANSECT

The application of the kinematic solution to the eastern transect is very similar to that used for the western transect (Morgan *et al.* 1994). The complicated geometry of the trench and prism toe along the eastern transect, and the geographically restricted physical property data sets, prevent the calculation of strains from directly obtained vertical thickness and volume ratios. Instead, the data are used to guide the development of reasonable solutions which are constrained to meet specific criteria. These include the following: (1) the distribution of input ratios should be smooth and continuous within a continuous domain, (2) the vertical thickness ratios and volume ratios within a continuous domain will generally decrease downward, a consequence of the dominant effects of gravitational consolidation, and (3) in the absence of erosion, the upper (seafloor) and lower (décollement) boundaries will approximate element streaklines within the nearly steady-state system for deposition and accretion.

An important test for the strain calculations lies in the reconstructed geometry of the section, determined from calculated element displacements. As prescribed by the boundary conditions, stratigraphic reflectors should be continuous across the restored thrust faults and the boundaries of the individual domains should match. In addition, in order to prevent unsubstantiated internal shear strains, initially vertical lines should remain approximately straight, thereby preserving the general shape of the individual domains. The above requirements demand an iterative approach to estimating strains, whereby the calculated solution is progressively improved by modifying the input distributions.

Vertical thickness ratios

The stratigraphic and structural geometries along the eastern transect are somewhat more complicated than along the western transect. The position of the deformation front is not as well defined. In addition, the vertical spacing between reflectors (bed thickness) in the trench is much more variable than to the west. Bed thickness is generally highest near the center of the bed and tapers off towards the edges, reflecting the parabolic shape of the trench floor (Fig. 2) and the uneven sedimentation rates across the trench. For this reason, it is difficult to accurately distinguish between the stratigraphic and tectonic components of bed thickness change within the prism.

Due to the lateral changes in depositional thickness, vertical thickness ratios, which relate the deformed and undeformed bed thicknesses, cannot be obtained directly from reflector spacing. Instead, vertical thickness ratios must be derived iteratively during the first

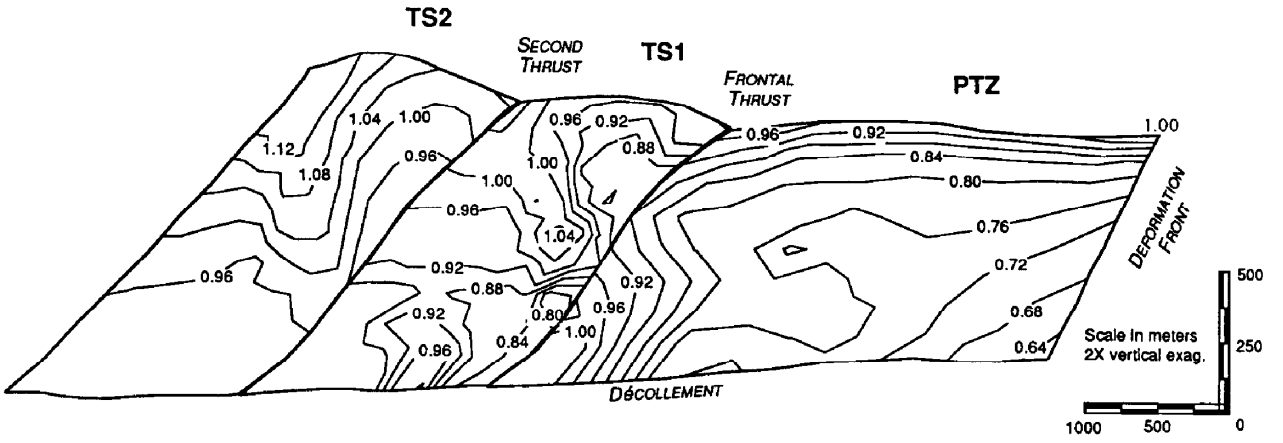

Fig. 4. Vertical thickness ratios. Smoothed vertical thickness ratios, roughly estimated from changes in vertical reflector spacing, and defined iteratively by fitting element streaklines to the stratigraphic reflectors and the geometry of the prism toe.

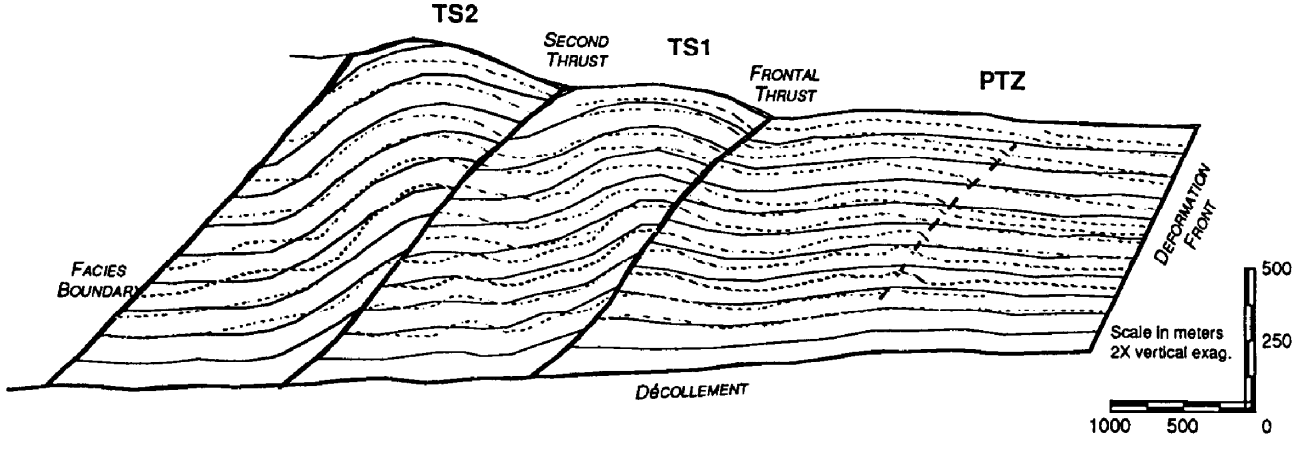

Fig. 5. Element streaklines. Element streaklines corresponding to the vertical thickness ratios in Fig. 4, fitted to the stratigraphic reflectors and the geometry of the prism toe. Streaklines are shown in solid lines, stratigraphic reflectors are dotted.

part of the kinematic solution, i.e. the calculation of vertical displacements and streaklines. Thus, the exercise becomes one of fitting the smooth streaklines to the geometries of the stratigraphic reflectors, constrained by the kinematic model shown in Fig. 3 and by the criteria stated above.

The resulting distribution of vertical thickness ratios (Fig. 4) is generally smooth within the PTZ, but deflected in response to the slight warping of the Shikoku basin strata below the incipient thrust fault. The uplift of beds within the footwall of the frontal thrust causes a significant increase in vertical thickness ratios, introducing nearly vertical contours. Contours of constant vertical thickness ratio are subparallel to streaklines within the uppermost strata, indicating relatively little tectonic change in thickness. Within the leading edge of the first thrust sheet, thickness ratios appear continuous with the upper part of the PTZ but offset across the fault. In the correlative position in the second thrust sheet, these ratios are somewhat higher. Vertical thickness ratios generally increase arcward along streaklines within individual domains, reaching their highest values within the footwalls of the thrust faults. The derived streaklines (Fig. 5) are approximately parallel to the Shikoku Basin reflectors, but oblique to the trench fill reflectors, similar to the model in Fig. 3. The angles between the streaklines and trench fill reflectors vary with distance from the facies boundary, just as the dip of the reflectors varies along their length (Fig. 2).

Volume ratios

The determination of the volume ratio distribution for the eastern transect is more problematic than for the western transect. Along the western transect, the coincidence of several expanding spread profiles (ESPs; Stoffa *et al.* 1992) with DSDP drill Sites, 582 and 583, permitted the creation of a site specific velocity–porosity transform (Karig 1990). This could then be used to interpolate porosities for the other ESPs, yielding a reasonable two-dimensional porosity distribution (Morgan *et al.* 1994). Along the eastern transect, the only direct porosity control section in the toe of the prism is given by ODP Site 808, which unfortunately does not coincide with any of several split-spread profiles (SSPs) collected along the transect (Stoffa *et al.* 1992). Velocity–porosity transforms derived from the sparse velocity logs and vertical seismic data (e.g. Hyndman *et al.* 1993) also prove to be of limited value for resolving the two-dimensional poro-

sity distribution. Moreover, the dependence of seismic velocities on poorly quantified material properties such as cementation, sediment anisotropy and microcracking, make the use of such a universal transform suspect (Bourbié *et al.* 1987, Lewis 1991, Karig 1993).

Due to the uncertainties in the velocity-derived porosities, the scanty porosity and velocity data were used to develop a limiting volume distribution. Porosities collected from ODP Site 808 (Taira *et al.* 1991) provided a control section within the prism, while the upper portion of the porosity profile collected from DSDP Site 582 (Bray & Karig 1985) served as an undeformed analog in the trench. As lateral changes in porosity are poorly constrained at depth, we choose to fix the volumes of sediment elements accreted along the base of the prism (i.e. the décollement) to be constant. The two-dimensional volume distribution was then modified as the diffuse strain field was determined iteratively using the criteria given above.

Realistically, it is more reasonable to believe that there has been some dewatering along the base of the prism, due in part to the increased overburden during tectonic thickening and to the increase in tectonic stresses. Porosity was observed to change along the base of the western transect, although this change was comparatively small (Morgan *et al.* 1994). Dewatering along the eastern transect is also supported by a 5–8% downward increase in porosity across the décollement at ODP Site 808 (Taira *et al.* 1991). Nevertheless, the constant volume assumption along the base leads to diffuse strain calculations which minimize the amount of horizontal shortening within the prism toe, providing a limiting solution.

Shipboard porosities were corrected back to *in situ* conditions by accounting for porosity rebound during unloading, and adjusting for the poorly sampled sand component. Porosity rebound estimates for the clay component were obtained from deformation experiments on cores form Hole 808 (Karig 1993 and unpublished data), yielding lower rebound estimates than those proposed by Hamilton (1976). Sand porosities were assumed to vary only slightly with depth, as suggested by experiments (Karig & Hou 1992). Based on limited logging results and general stratigraphic trends (Taira *et al.* 1991), the percentage of sand in the hole was determined to decrease nonlinearly downhole from about 50% at the very top to about 25% at the base of the trench fill, and 0% within the more uniform Shikoku hemipelagites.

The *in situ* porosity curve obtained from Site 808, compared with that derived by Karig (1990) for Site 582 (Fig. 6), demonstrates a slight arcward decrease in porosity, at least near the surface. The tectonically undeformed analog provided by Site 582 constrains the initial porosity at the trench floor, η_0, to be 56%, compared to about 48% inferred at the top of Site 808. Immediately above the décollement, porosities are estimated at 27% from ODP Site 808.

Volume ratios are calculated from the corrected porosities according to

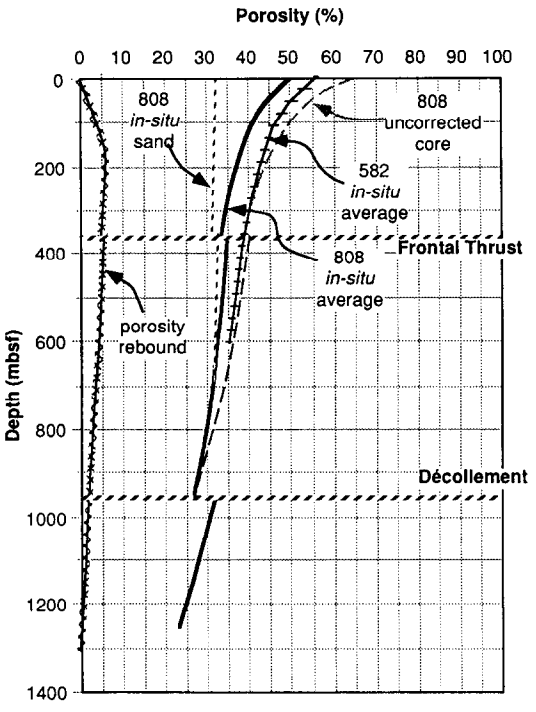

Fig. 6. *In situ* porosities vs depth. *In situ* porosities for ODP Site 808 (bold line), calculated from shipboard porosities and corrected for the sand component and porosity rebound. This curve is compared with the reference *in situ* porosity curve for DSDP Site 582 in the trench (horizontally dashed), derived by Karig (1990). Uncorrected shipboard porosities are dashed, rebound estimates are cross-hatched, and porosities for the sand component are indicated by the dotted line. (Shipboard physical properties data presented for Hole 808 (Taira *et al.* 1991) were not internally consistent; porosities calculated from the water content were uniformly higher than those calculated from the bulk densities.) We used porosities recalculated based on the tabulated bulk and grain densities.

$$\frac{V}{V_0} = \frac{1-\eta_0}{1-\eta} \tag{2}$$

where η represents the final porosity. The resulting distribution of volume ratios is shown in Fig. 7. A maximum ratio of 1.0 is observed at the trench floor. Minimum volume ratios of 0.62 are estimated along the base of the prism. Volume ratios decrease arcward along the seafloor to about 0.85 just in front of the frontal thrust. Contours of constant volume ratios cross element streaklines high in the section while they follow streaklines at depth. This argues for significant dewatering near the surface where the sediments are relatively unconsolidated, and less within the more consolidated sediments at depth. This is consistent with the findings along the western transect (Morgan *et al.* 1994).

Volume ratios near the top of Hole 808C in TS1 are about 0.78, corresponding to a surface porosity of about 43%. This is less than indicated in Fig. 6, but the discrepancy may be partially explained by scatter in the measured porosity data or by anomalously high porosities in the remobilized sediments at the top of the hole. Maximum volume ratios within TS2 reach 0.76, or a porosity of about 41%. Volume ratio distributions are discontinuous across both thrust faults, reflecting the juxtaposition of lower porosity

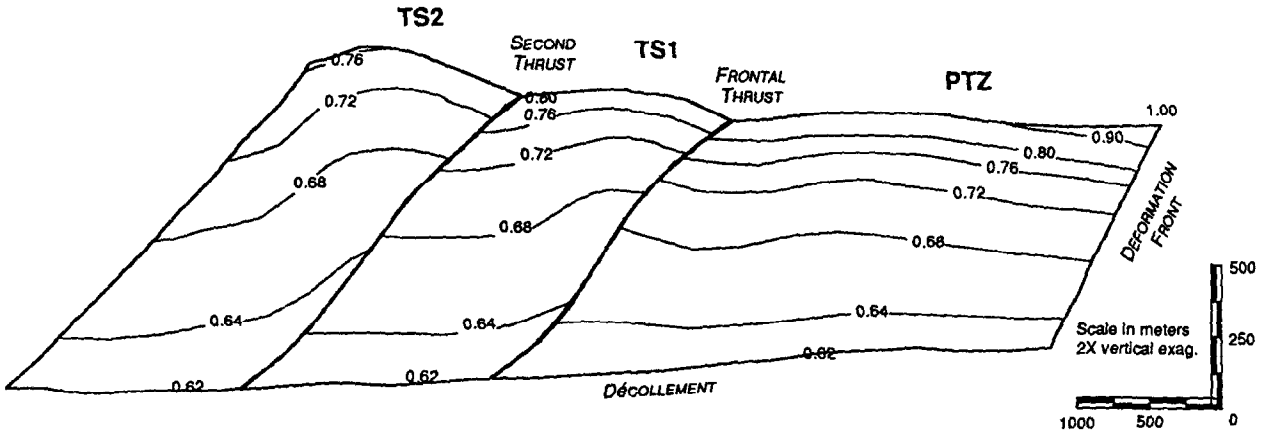

Fig. 7. Volume ratios. Volume ratios derived prism toe from corrected *in situ* porosities for Site 808 (Fig. 6), and a limiting strain condition assuming no volume change along the décollement. The final volume ratio distribution was determined iteratively as the diffuse strain field was calculated, based on the criteria given in the text.

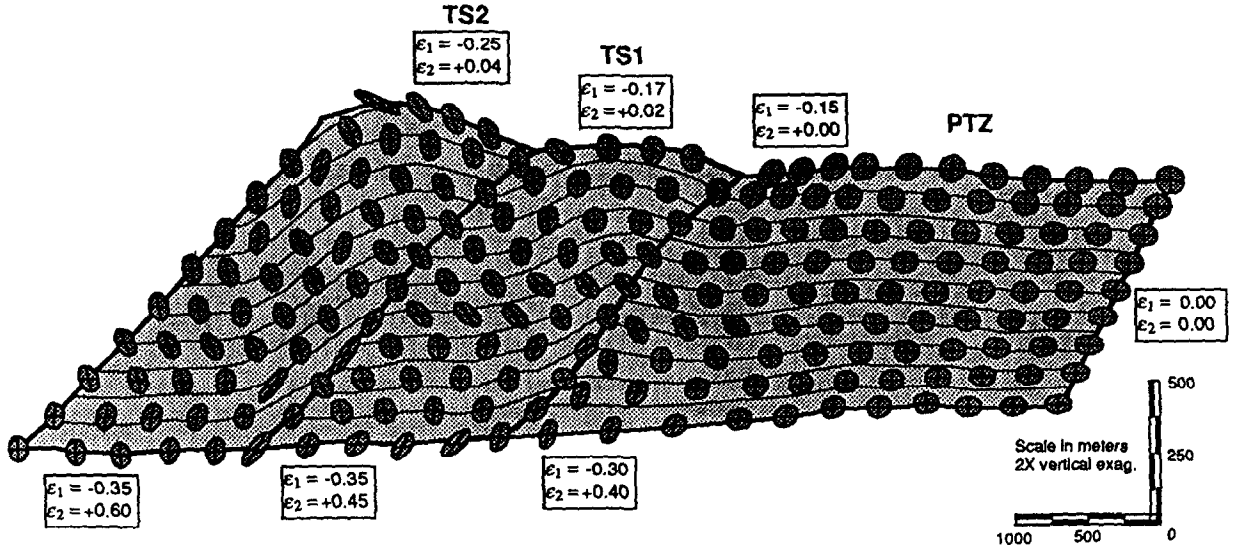

Fig. 8. Distribution of strains. Calculated strain ellipses are plotted with element streaklines. Superimposed on the strain ellipses are line elements that were initially horizontal and vertical in the undeformed configuration. Average horizontal and vertical tectonic strains (ε_1 and ε_2, respectively) are also shown near the top and the base of the prism. Near-surface sediments show little vertical extension. Deeper sediments show significant extension, particularly in the trailing edges of the protothrust zone and the thrust sheets. Shear strains are not well resolved in this analysis, introducing irregular rotations of the strain ellipses.

sediments in the hangingwall against higher porosity sediments in the footwall.

STRAIN DISTRIBUTION

Our numerical approach, constrained by the assumptions given above, yields a solution for the deformation state within the protothrust zone and the first two thrust sheets. On the gross scale, there appears to be a continuous variation with depth in the amount of volume change and vertical extension an element incurs in response to horizontal shortening. Superimposed on this flattening field are folding and shearing associated with displacement along the thrust faults. Larger-scale heterogeneities also occur in the strain pattern, reflected by high vertical thickening and horizontal shortening within the trailing edges of the domains.

Calculated strain ellipses, representing transformed unit circles in the undeformed reference configuration (at the seafloor), are used to display the main results (Fig. 8). As an indication of the magnitudes of the strain distribution, horizontal and vertical tectonic strains (ε_1 and ε_2, respectively) are also given for representative positions within the prism. The results show several trends: (1) strain ellipses generally flatten with depth, reflecting increasing compaction due to burial in the trench; (2) throughout the PTZ and within the untilted beds in the thrust sheets, horizontal flattening without significant rotation is demonstrated; (3) generally, deeper material elements show considerable extension in response to horizontal shortening, with little change in volume; those near the surface dewater as they shorten horizontally, without much vertical extension; and (4) within the trailing edges of the thrust sheets (at least TS1) and the PTZ, strain ellipses demonstrate significantly greater horizontal shortening and vertical extension than observed along correlative streaklines

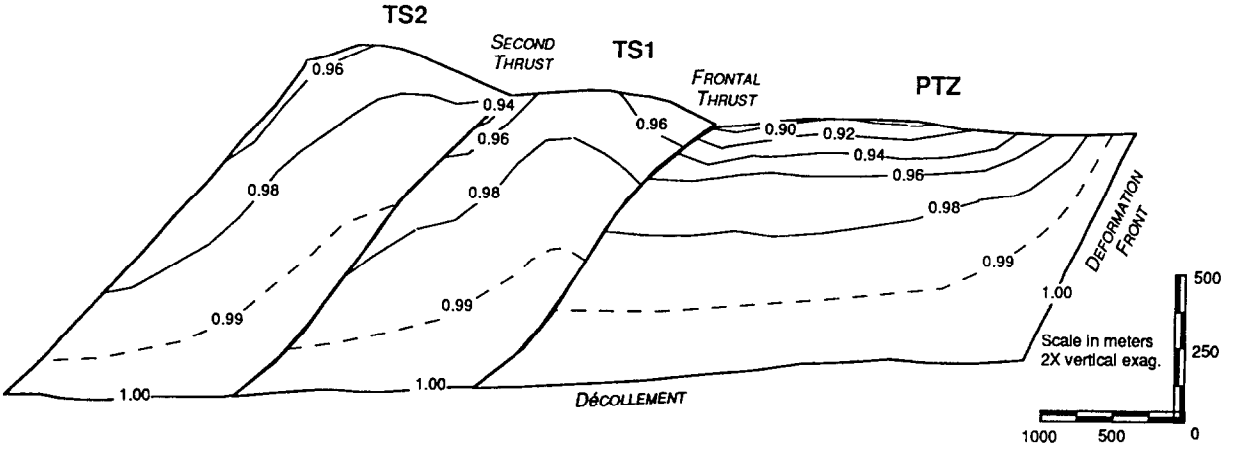

Fig. 9. Tectonic volume ratios. Tectonic volume ratios resolved along streaklines show the greatest volume change near the seafloor, and the least at depth. The steepest gradient is observed near the deformation front.

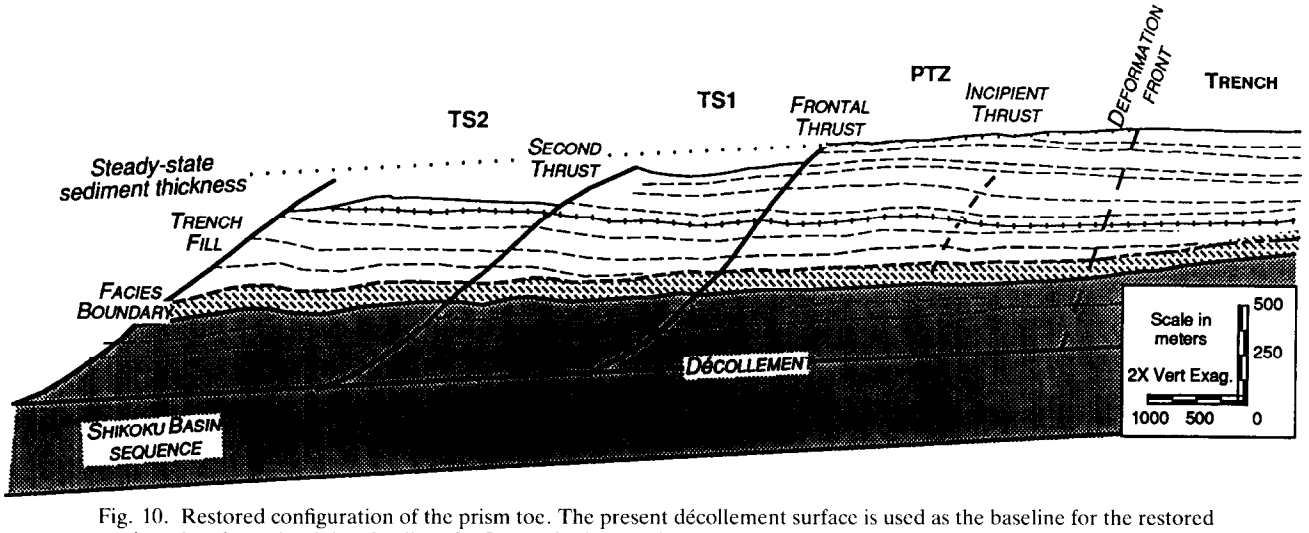

Fig. 10. Restored configuration of the prism toe. The present décollement surface is used as the baseline for the restored section, thereby maintaining the dips of reflectors in the trench. Restored sediment thicknesses represent the uncompacted thickness of the sediment package as it passed through the deformation front. Due to simultaneous sediment consolidation and arcward migration, the upper surface of the restored prism dips; if the accreted sediment thickness were constant, then the restored surface (dotted line) would parallel the décollement surface. The apparent loss of the uppermost reflectors in the thrust sheets is attributed to submarine erosion.

within the leading edges of the thrust sheets. Again, this arcward increase in strain reflects the very heterogeneous nature of strain within individual thrust sheets.

Strain ellipses within the tilted beds in the hangingwall folds in TS1 and TS2 would typically demonstrate significant shear strain associated with bed-parallel slip. However, horizontal shear strains prove to be very sensitive to variations in the volume ratio distribution, and consequently are poorly resolved in this kinematic solution (Morgan *et al.* 1994). The resulting oscillations in strain ellipse orientation thus are not representative of material strains. Nevertheless, the effect of this instability on the calculation of element displacements appears to be small.

The tectonic strains and volume changes incurred arcward of the deformation front can be obtained by decomposing **F** along element streaklines (Morgan *et al.* 1994). Tectonic volume ratios (Fig. 9) show the greatest tectonic dewatering in the uppermost sediments, and the least near the base of the prism as demanded by the input. The steepest gradient in volume is observed near the deformation front.

RESTORED SECTION

In addition to calculating total and tectonic finite strains, our kinematic solution yields element co-ordinates in the reference configuration, thereby permitting the reconstruction of an undeformed cross-section across the toe of the Nankai prism (Fig. 10). This reconstruction removes both tectonic strains accrued arcward of the deformation front and uniaxial compaction incurred within the trench and Shikoku Basin. The geometry of the resulting cross-section is somewhat unusual, and never existed during the history of the prism. We have reconstructed the deformed strata using its uncompacted thickness.

The origin of the reconstructed configuration is defined at the intersection of the deformation front and décollement, and horizontal co-ordinates are given relative to this reference. The restored section is plotted using the décollement as a baseline, thus maintaining the geometry of the trench and the underlying strata and preserving the dips of reflectors within the trench. Vertical co-ordinates are defined by the vertical positions of

elements relative to the décollement, with the sediment compaction removed (a restored porosity of about 56%). Uplift at the deformation front caused the accumulation of sediment to cease, thus the restored surface of the prism slopes arcward while the trench floor remains flat. The subhorizontal trench reflectors will be truncated at this surface. If the width of the trench and the thickness of the accreting section had been uniform through time, then the top of the restored section would follow the upper dotted line which parallels the décollement surface. The downward steps across the thrust fault boundaries at the top of the section are believed to result from submarine erosion, which removed the uppermost reflectors in TS1 and TS2.

The undeformed configuration of the key reflectors used in this study (Fig. 10) sheds light on the depositional history at the Nankai convergent margin, defining the geometry of the depositional surface at a given time. Beds within the Shikoku Basin sequence, lying below the facies boundary (emboldened) are generally subparallel to the décollement surface, although local undulations arise from the inexact fit of streaklines. Dips of the trench fill reflectors are more variable, with the deepest beds nearly parallel to the facies boundary and the shallower beds more oblique. This reflects the non-uniform sedimentation associated with fan turbidites, and the parabolic shape of the floor of the trench (Fig. 2). In the simple depositional model presented before (Fig. 3), trench-fill reflectors onlap the facies boundary, as they do near the center of the first thrust sheet. However, throughout much of the section, the trench reflectors nearly parallel the facies boundary and the underlying strata. This suggests that there may have been temporal variations in the width of the trench and the position of the outer trench margin, possibly due to non-uniform turbidity flows. Alternatively, these reflectors may mark regionally extensive isochronous events (e.g. ash deposits) which blanket both trench and basin, one possible explanation for the sharp reflector (marked 'isochron') which crosses the facies boundary in Fig. 2.

The geometry and dimensions of the reconstructed PTZ and thrust sheets can be used to evaluate the plausibility of our strain calculations. In the deformed state, the progression of thrust faults observed on the deformed section, including the incipient thrust within the PTZ, show similar listric geometries with average dips of 30–35°. In the restored configuration (Fig. 13), fault dips tend to shallow in the arcward direction. The change in initial dip of the three thrust faults may be real, and the similar geometries in the current configuration a consequence of the arcward steepening of faults as new seaward thrusts form. This would argue for a progressive change in the mechanical conditions of faulting, and a fortuitous coincidence of fault dips today. However, if the controls on fault shape can be argued to be time-independent (steady-state), then the calculated distribution of horizontal shortening within the thrust sheets may have been over-estimated within the deepest sediments or under-estimated within the shallowest.

The deformed widths of the thrust sheets on the seismic depth section (Fig. 2) decrease slightly in the arcward direction, a phenomenon noted previously along both transects and attributed to internal shortening and folding of the thrust package (Karig 1985, Moore *et al.* 1991). However, the restored widths of the thrust sheets increase arcward. An arcward increase in thrust sheet width across the section is corroborated by an increase in the lengths of individual deformed reflectors within successive thrust sheets. Thrust fault spacing has previously been correlated with changes in stratigraphic thickness (e.g. Goff & Wiltschko 1992), suggesting that the accreted thickness of the trench sediments has decreased through time (Karig & Angevine 1985). It is possible that the variations in stratigraphic thickness also mechanically control the initial dip of the thrust faults.

A comparison of the deformed and undeformed configurations of the PTZ and the first two thrust sheets yields preliminary estimates for horizontal shortening in the prism toe. The difference in total length between the two states indicates a total horizontal shortening of about 3.3 km, or about 31% of the initial length of 10.5 km. As our results represent a limiting solution corresponding to no volume change along the base of the prism, this shortening estimate is a minimum value. By comparison, simply retrodeforming the folded and displaced strata along the faults recovers only about 1.1 km of shortening. Thus, about 68% (minimum) of the total shortening can be attributed to diffuse, internal strain. This represents a substantial contribution which must be factored into shortening and convergence estimates.

KINEMATIC HISTORY AND MECHANICAL CONSIDERATIONS

The heterogeneous strain distribution in the Nankai prism toe appears to be controlled by at least two factors: (1) the initial consolidation state which affects the strain response, and (2) the position of material relative to thrust faults. The first factor, also recognized within the PTZ along the western transect (Morgan *et al.* 1994), results in a continuous balance between the vertical thickening and volume change which accompanies horizontal shortening. The more consolidated material near the base of the prism displays nearly constant-volume, distortional strain, while the more porous sediments near the surface dewater with little vertical extension. The importance of position of the accreted material relative to the thrust faults is indicated by the comparatively high distortional strains found in the footwalls of the thrust faults relative to the hangingwalls.

The difference in strain state across the thrust faults is suggested by the seismic profiles as well (Fig. 2). Beds within the footwalls of the thrust faults tend to be considerably thicker than correlative strata in the hangingwall, at least across the frontal thrust and the incipient fault in the PTZ. In addition, there is a contrast in seismic coherence across the thrust faults, probably

due to the internal disruption of the footwall sediments. The high strains in the trailing edges of thrust sheets also complicate the geometries of the folded strata within the thrust sheets. Bed-normal thickening of the flat-lying beds in the trailing edges of the thrust sheets prevents the deformation being restored simply by unfolding and displacing the strata. In addition, differential thickening across the thrust faults results in fault displacements which vary along the length of the fault. Bed offsets are greatest near the center of the fault and decrease both upwards and downwards.

One possible explanation for the apparently high strains in the trailing edges of the thrust sheets is the faulting of previously folded beds, and the truncation of the steeply dipping limb along the fault. This possibility is supported by the presence of folded Shikoku Basin strata beneath the incipient fault in the PTZ. Such a model may help to explain the shallow dips of the kink planes defining the folds within the thrust sheets. Instead of forming and migrating as the fault-bend fold develops along the thrust ramp, kink planes associated with a pre-existing fold may have rotated to shallower angles during displacement along the fault. The absence of folded stata within the footwall of the second thrust fault, however, suggests that this model may not apply universally.

An alternative explanation for the differential strains across the thrust faults may be the preferential thickening of footwall sediments relative to the hangingwall after thrusting. Deformation structures and fabrics in cores recovered from ODP Site 808 lend support to the idea that the mode and distribution of deformation in the toe of the prism are not uniform (Taira *et al.* 1991, Maltman *et al.* 1993). Discrete structures (faults and deformation bands) were completely absent above 260 m below the seafloor (mbsf) and unevenly distributed below this depth. Microfaults generally increased in frequency downhole to the décollement, with major concentrations about the frontal thrust and décollement. Significant clusters occurred within the PTZ between the frontal thrust and the décollement zone, but these were not obviously related to zones of shear. Deformation bands, composed of anastomosing kink and shear bands (Karig & Lundberg 1990), appeared to be nearly symmetrically disposed about the frontal thrust. Although the data set is limited, the high concentrations of brittle faults in ODP Hole 808C appear to correspond to regions of bed thickening and decreased seismic coherence in the footwalls of the thrust faults. These areas also represent zones of relatively low volume loss and high distortion in our kinematic solution, suggesting that such high strains are dominantly accommodated by brittle deformation.

Indicators for pervasive ductile strains accompanying tectonic deformation are less obvious than the brittle and semi-brittle structures, although ductile modes may be important contributors to total diffuse deformation. Fabric analyses in cores from ODP Hole 808C appear to indicate that some tectonic shortening is accommodated by mineral realignment (Morgan & Karig 1933, Owens 1993). Preliminary estimates suggest that pervasive ductile horizontal shortening reaches 10%, and varies little with depth above the décollement (Morgan & Karig 1993). By comparison, diffuse strain estimates obtained in our kinematic solution suggest about 15% horizontal shortening in the hangingwall of the frontal thrust and about 30% in the footwall (Fig. 8).

The differences between diffuse and ductile strains provide crude estimates for the non-ductile contribution to tectonic shortening. About 5% horizontal shortening in the hangingwall, and about 20% in the footwall may be due to brittle or semi-brittle strains. The absence of discrete structures in the upper portion of Hole 808C and the relatively high seismic coherence in the leading edges of the thrust sheets support minimal brittle deformation in these regions. The high estimates for brittle strains in the footwall are consistent with the increased abundance of microfaults in Hole 808C below the frontal thrust. Clearly, the various deformation modes vary in importance with position, suggesting that significant differences in mechanical condition may exist above and below the frontal thrust.

Differences in the mechanical state of sediments on either side of the frontal thrust can probably be attributed to loading and displacement along the active thrust fault. If the prism represents a strain-driven system, then the development of a throughgoing fault will tend to cause a decrease in the applied horizontal stress. In the hangingwall, sediments will experience no increase in vertical stress, and probably a decrease in vertical stress due to erosion. Thus differential stress ($\Delta\sigma$) and effective mean stress (σ'_m) will both drop, returning the sediment to the elastic field and preventing additional strain. It is more difficult to predict the mechanical state of sediments in the footwall. Initially, stresses induced by thrusting will likely cause a return to the elastic field as well. Vertical loading of the footwall will cause an increase in total vertical stress, tending to decrease $\Delta\sigma$ and maintain or slightly increase σ'_m. As fault-induced pore pressures dissipate, this trend will continue.

The brittle failure of sediments in the footwall requires an increase in $\Delta\sigma$ from this elastic state, such as might be induced by a sudden increase in pore pressure (e.g. Mandl 1988, equation 11.6–24b, p. 273). Pore pressure pulses may derive from a highly pressurized décollement (Karig *et al.* 1990) within a diffusive or microchannelized flow regime (e.g. Maltman *et al.* 1992, Kastner *et al.* 1993), concentrating brittle deformation along the base of the prism. Although supporting evidence was lacking at Site 808, transient pulses of high pore pressure along the frontal thrust faults may also localize brittle deformation there, particularly in sediments buried in the footwalls.

Integrating the patterns for diffuse strain with drill core evidence for deformation and preliminary mechanical results leads to a summary model for the evolution and distribution of deformation within the eastern Nankai prism toe (Fig. 11). The initial stages of deformation are believed to be ductile for sediments accreted at all depths, leading to critical state failure very close to the

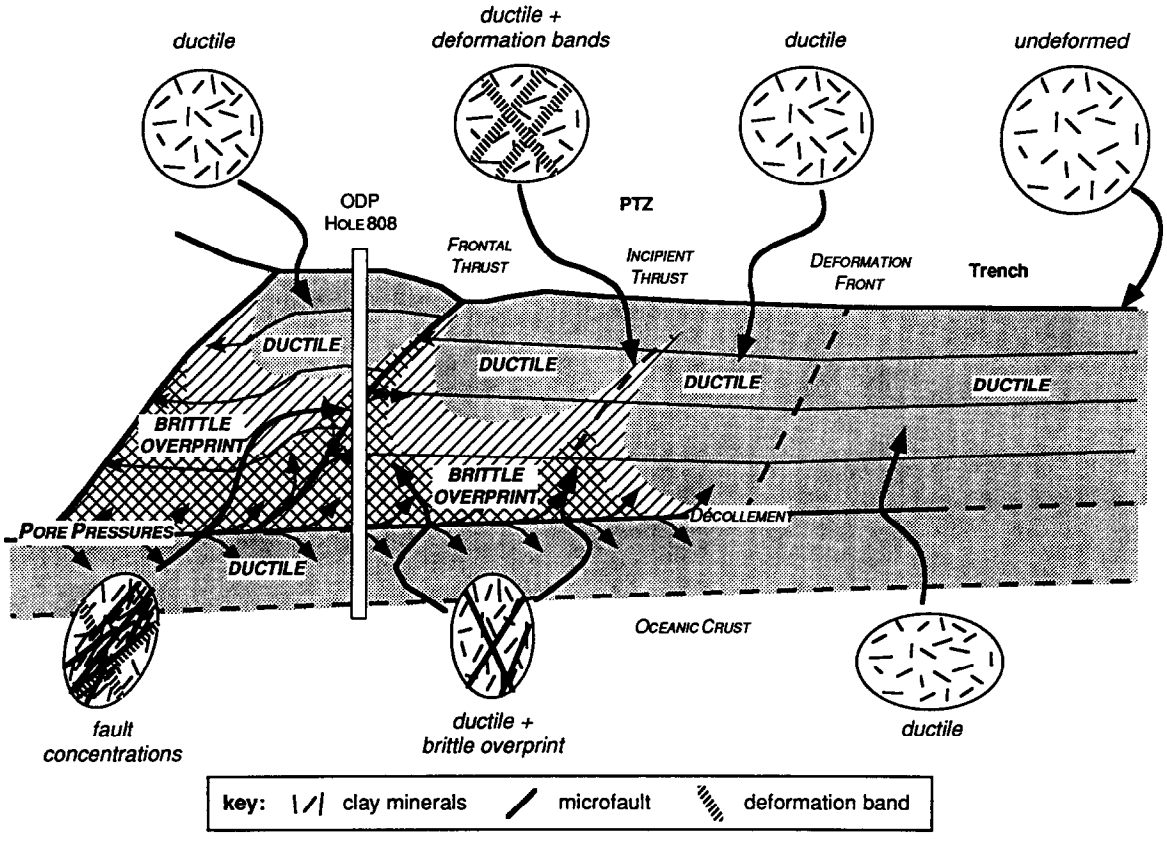

Fig. 11. Distribution of ductile and brittle strains in the toe of the eastern Nankai prism. Initial tectonic strains are ductile (shaded) near the deformation front. Brittle deformation (cross-hatched) overprints this ductile strain field near the base of the prism, and eventually around initiating or existing thrust faults. These brittle strains may arise from high pore pressures diffusing away from the décollement and the frontal thrust fault. Strain ellipses demonstrate the estimated finite strain state, and the relationships between deformation structures and fabrics inferred from diffuse strain calculations, deformation structures observed in ODP drill cores, clay mineral fabrics, and sediment porosities. (Modified from Karig & Morgan in press.)

deformation front. Subsequently, high pore pressures diffusing away from the décollement may localize brittle faults near the base of the prism, overprinting the primary ductile fabric and leading to relatively high distortion (vertical extension, horizontal shortening) in the deeper sediments. Sediments higher in the section may generally remain in the ductile field, although local instabilities may result in the formation of tight folds and semi-ductile deformation bands (e.g. Karig & Morgan in press). Concentrations of these features, associated weakening of the sediments, and induced high pore pressures, may lead to local microfaulting and ultimately the formation and propagation of throughgoing thrust faults. Uplifted and eroded sediments in the hangingwall of the faults probably see little additional deformation, while footwall sediments may experience increased microfaulting.

Decreasing offset towards the ends of the thrust faults and the discontinuous incipient thrust fault in the PTZ suggest that throughgoing thrust faults may initiate well above the décollement and propagate both upwards and downwards (e.g. Eisenstadt & DePaor 1987, Ellis & Dunlap 1988, Goff & Wiltschko 1992). This may result from local stress or strain conditions within the prism, possibly related to mechanical boundaries or pore pressure concentrations (Goff & Wiltschko 1992).

CONCLUSIONS

Our analysis has delineated a distribution of diffuse deformation for the toe of the eastern Nankai accretionary prism that demonstrates significant variability in magnitude. Much of this heterogeneity appears to result from the structural position of the sediment as much as from the initial consolidation state. The general deformation field is one in which deeper sediments reflect high vertical extension incurred through either ductile or brittle deformation, and shallower sediments display significant dewatering and dominantly ductile strain in response to horizontal shortening. This distribution of strain is perturbed by local zones of high strains apparently resulting from small-scale distributed brittle faulting, probably due to the combination of burial beneath thrust faults and high pore pressures at depth. The results detail a sequence of deformation that progresses from pervasive ductile deformation accomplished by grain boundary sliding, through localized ductile failure and the formation of deformation bands, and finally to brittle faulting. The timing of the formation of the large scale thrust fault relative to the distributed core-scale faults at the base of the prism can only be partially constrained.

There is clear evidence for continued horizontal short-

ening within the deforming thrust sheets, but mostly restricted to the trailing edges. This strain differential within thrust sheets is best explained by variations in mechanical conditions associated with thrusting; uplifted and eroded sediments within the hangingwalls may cease to deform; the relatively weaker sediments buried in the footwalls may continue to deform, primarily brittlely due to high pore pressures diffusing away from a pressurized décollement.

Perhaps the most important result of this study is the development and demonstration of a new technique for balancing and restoring deformed sections, allowing us to examine the depositional and deformational history of the accretionary margin. Our calculations suggest that up to 68% of the total shortening of 3.3 km is due to diffuse internal deformation. Although the calculated strain field does not represent a unique solution, it defines a plausible solution. We can predict the undeformed configuration of the margin, and identify depositional patterns complicated by non-uniform turbidite sedimentation within the trench and temporal variations in the position of the outer trench margin. Although the application of our kinematic solution has been presented here for the specific example of the Nankai accretionary margin, it should be valid in other domains, particularly where volumetric strain is an important factor. With the appropriate data set, this method may be equally useful for three-dimensional analyses, offering a rigorous approach to evaluating complexly deformed terrains.

Acknowledgements—The thoughtful comments and queries offered by Peter Hudleston and two anonymous reviewers guided the authors to write a much clarified manuscript. Much of this work was supported by a fellowship offered to Morgan by the Shell Foundation, and by NSF Grant OCE-9202784.

REFERENCES

Borradaile, G. J. 1981. Particulate flow of rock and formation of cleavage. *Tectonophysics* **72**, 305–321.

Bourbié, T., Coussy, O. & Zinszner, B. 1987. *Acoustics of Porous Media*. Éditions Tecnip, Paris.

Bray, C. J. & Karig, D. E. 1985. Physical properties of sediments from the Nankai Trough, Deep Sea Drilling Project Leg 87A, Sites 582 and 583. In *Init. Repts, DSDP* (edited by Kagami, H., Karig, D. E., Coulbourn, W. T. *et al.*). (U.S. Govt. Printing Office) Washington, **87**, 827–842.

Bray, C. J. & Karig, D. E. 1988. Dewatering and extensional deformation of the Shikoku Basin hemipelagic sediments in the Nankai Trough. *Pure & Appl. Geophys.* **128**, 725–247.

Byrne, T., Brückmann, W., Owens, W., Lallemant, S. & Maltman, A. 1993. Structural synthesis: correlation of structural fabrics, velocity anisotropy, and magnetic susceptibility data. In: *Proc. ODP, Sci. Results* (edited by Hill, I., Taira, A., Firth, J. *et al.*). College Station, Tex. **B131**, 365–378.

Eisenstadt, G. & De Paor, D. G. 1987. Alternative model of thrust-fault propagation. *Geology* **15**, 630–633.

Ellis, M. A. & Dunlap, W. J. 1988. Displacement variation along thrust faults: Implications for the development of large faults. *J. Struct. Geol.* **10**, 183–192.

Goff, D. & Wiltschko, D. V. 1992. Stresses beneath a ramping thrust sheet. *J. Struct. Geol.* **14**, 437–449.

Hamilton, E. L. 1976. Variations of density and porosity with depth in deep sea sediments. *J. Sed. Pet.* **46**, 280–300.

Hill, I., Taira, A. & Firth, J. *et al.* 1993. *Proc. ODP, Sci. Results*. College Station, Texas **B131**.

Hyndman, R. D., Moore, G. F. & Moran, K. 1993. Velocity, porosity, and pore-fluid loss from the Nankai subduction zone accretionary prism. In: *Proc. ODP, Init. Repts* (edited by Hill, I., Taira, A., Firth, J. *et al.*). College Station, Texas **B131**, 211–220.

Kagami, H., Karig, D. E., Coulbourn, W. T. *et al.* 1985. *Init. Repts. DSDP* (U.S. Govt. Printing Office) Washington, **87**.

Karig, D. E. 1985. The framework of deformation in the Nankai Trough. In: *Init. Repts, DSDP* (edited by Kagami, H., Karig, D. E., Coulbourn, W. T. *et al.*). (U.S. Govt. Printing Office) Washington, **87**, 927–940.

Karig, D. E. 1990. Experimental and observational constraints on the mechanical behavior in the toes of accretionary prisms. In: *Deformation Mechanisms, Rheology and Tectonics* (edited by Knipe, R. J. & Rutter, E. H.). *Geol. Soc. Spec. Pub.* **54**, 383–398.

Karig, D. E. 1993. Reconsolidation tests and sonic velocity measurements of clay-rich sediments from the Nankai Trough. In: *Proc. ODP, Init. Repts* (edited by Hill, I., Taira, A., Firth, J. *et al.*). College Station, Texas **B131**, 247–260.

Karig, D. E. & Angevine, C. L. 1985. Geologic constraints on subduction rates in the Nankai Trough. In: *Init. Repts, DSDP* (edited by Kagami, H., Karig, D. E., Coulbourn, W. T. *et al.*). (U.S. Govt. Printing Office) Washington, **87**, 789–796.

Karig, D. E. & Hou, G. 1992. High-stress consolidation experiments and their geologic implications. *J. Geophys. Res.* **97**, 289–300.

Karig, D. E., Ingle, J. C. Jr., *et al.* 1975. *Init. Repts, DSDP* (U.S. Govt. Printing Office) Washington, **31**.

Karig, D. E. & Lundberg, N. 1990. Deformation bands from the toe of the Nankai accretionary prism. *J. Geophys. Res.* **95**, 9099–9109.

Karig, D. E., Moran, K. & Leg 131 Scientific Party. 1990. A dynamically sealed décollement: Nankai Prism. *EOS. Trans. Am. geophys. Union* **71**, 1626.

Karig, D. E. & Morgan, J. K. In press. Stress paths and strain histories during tectonic deformation of sediments. In: *Geological Deformation of Sediments* (edited by Maltman, A.). Chapman & Hall, London.

Kastens, K. A., Breen, N. A. & Cita, M. B. 1992. Progressive deformation of an evaporite-bearing accretionary complex: SeaMARC I, SeaBeam and piston-core observations from the Mediterranean Ridge. *Mar. geophys. Res.* **14**, 249–298.

Kastner, M., Elderfield, H., Jenkins, W. J., Gieskes, J. M. & Gamo, T. 1993. Geochemical and isotopic evidence for fluid flow in the western Nankai subduction zone, Japan. In: *Proc. ODP, Sci. Repts* (edited by Hill, I., Taira, A., Firth, J. *et al.*). College Station, Texas **B131**, 397–413.

Lewis, B. T. R. 1991. Changes in P and S waves caused by subduction related sediment accretion off Washington/Oregon. In: *Shear Waves in Marine Sediments* (edited by Hovem, J. M. *et al.*). Kluwer Academic Publishers.

Maltman, A. 1984. On the term 'soft-sediment deformation'. *J. Struct. Geol.* **6**, 589–592.

Maltman, A., Byrne, T., Karig, D., Lallement S. & Leg 131 Shipboard Party. 1992. Structural geological evidence from ODP Leg 131 regarding fluid flow in the Nankai prism, Japan. *Earth Planet. Sci. Lett.* **109**, 463–468.

Maltman, A., Byrne, T., Karig, D., Lallement, S., Knipe, R. & Henry, P. 1993. Deformation structures at Site 808, Nankai accretionary prism, Japan. In: *Proc. ODP, Sci. Repts* (edited by Hill, I., Taira, A., Firth, J. *et al.*). College Station, Texas **B131**, 123–133.

Mandl, G. 1988. *Mechanics of Tectonic Faulting: Models and Basic Concepts*. Elsevier, Amsterdam.

Moore, G. F., Karig, D. E., Shipley, T. H., Taira, A., Stoffa, P. L. & Wood, W. T. 1991. Structural Framework of the ODP Leg 131 area, Nankai Trough. In: *Proc. ODP, Init. Repts* (edited by Taira, A., Hill, I., Firth, J. *et al.*). College Station, Texas **A131**, 15–20.

Moore, G. F., Shipley, T. H., Stoffa, P. L., Karig, D. E., Taira, A., Kuramoto, S., Tokuyama, H. & Suyehiro, K. 1990. Structure of the Nankai Trough accretionary zone from multichannel seismic reflection data. *J. Geophys. Res.* **95**, 8753–8765.

Morgan, J. K. & Karig, D. E. 1993. Ductile strains in clay-rich sediments from Hole 808C: Preliminary results using X-ray pole figure goniometry. In: *Proc. ODP, Sci. Repts* (edited by Hill, I., Taira, A., Firth, J. *et al.*). College Station, Texas **B131**, 141–155.

Morgan, J. K., Karig, D. E. & Maniatty, A. 1994. The estimation of diffuse strains in the toe of the western Nankai accretionary prism: A kinematic solution. *J. geophys. Res.*

Owens, W. H. 1993. Remanence and magnetic fabric studies of samples from Hole 131-808C, Nankai Trough. In: *Proc. ODP, Sci. Repts* (edited by Hill, I., Taira, A., Firth, J. *et al.*). College Station, Texas **B131**, 301–310.

Peerless, S. J. 1967. *Basic Fluid Mechanics*. Pergamon Press, Oxford.

Shipboard Scientific Party. 1991. Geological background and objectives. In: *Proc. ODP, Init. Repts* (edited by Taira, A., Hill, I., Firth, J. *et al.*). College Station, Texas **A131**, 5–14.

Stoffa, P. L., Wood, W. T., Shipley, T. H., Moore, G. F., Nishiyama, E., Botelho, M. A. B., Taira, A., Tokuyama, H. & Suyehiro, K. 1992. Deepwater high-resolution expanding spread and split spread seismic profiles in the Nankai Trough. *J. geophys. Res.* **97**, 1687–1713.

Suppe, J. 1983. Geometry and kinematics of fault-bend folding. *Am. J. Sci.* **283**, 684–721.

Taira, A., Hill, I. Firth, J. *et al.* 1991. *Proc. ODP, Init. Repts*. College Station, Texas **A131**.

Wood, D. M. 1990. *Soil Behavior and Critical State Soil Mechanics*. Cambridge University Press, Cambridge.

Woodward, N. B., Boyer, S. E. & Suppe, J. 1985. An outline of balanced cross-sections. U. Tenn., Dept. Geol. Sci., *Studies in Geology* **11**.